Research on Engineering Structures & Materials
www.jresm.org
Research Group

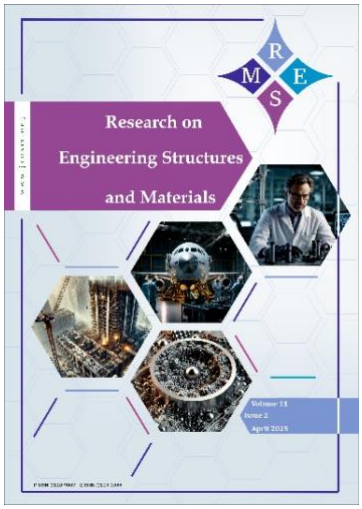

Impact of the evolution of the RPA 2024 seismic code and major earthquakes on the seismic response of self-stable reinforced concrete buildings

Abdellah Boudina, Salem Merabti, Smain Benyamina, Abdelheq Guettiche, Rachid Chadouli

Online Publication Date: 30 November 2025

URL: http://www.jresm.org/archive/resm2025-1070ea0808rs.html
DOI: http://dx.doi.org/10.17515/resm2025-1070ea0808rs

Journal Abbreviation: *Res. Eng. Struct. Mater.*

To cite this article
Boudina A, Merabti S, Benyamina S, Guettiche A, Chadouli R. Impact of the evolution of the RPA 2024 seismic code and major earthquakes on the seismic response of self-stable reinforced concrete buildings. *Res. Eng. Struct. Mater.*, 2026; 12(3): 1787-1805.

Research on Engineering Structures & Materials
www.jresm.org
MIM Research Group

Research Article

Impact of the evolution of the RPA 2024 seismic code and major earthquakes on the seismic response of self-stable reinforced concrete buildings

Abdellah Boudina [*,1,a], Salem Merabti [2,b], Smain Benyamina [2,c], Abdelheq Guettiche [3,d], Rachid Chadouli [1,e]

[1]*Laboratory of Fluid Industrials, Measures & Application (FIMA), Faculty of Science and Technology, University Djilali Bounaama of Khemis-Miliana, 44225, Algeria*
[2]*Acoustics and Civil Engineering Laboratory, Faculty of Sciences and Technology, Khemis-Miliana University, Road of Theniet el Had, Khemis Miliana 44225, Algeria*
[3]*Environmental Engineering and Technology Laboratory, Institute of Science and Technology, University Center Abdelhafid Boussouf of Mila, 43000, Algeria*

Article Info

Article History:

Received 08 Aug 2025
Accepted 29 Nov 2025

Keywords:

Self-stable buildings;
Boumerdès earthquake;
Seismic responses;
RPA 1999 version 2003;
RPA 2024

Abstract

This article presents a multi-spectral and multi-normative analysis of the seismic response of self-stable reinforced concrete frame buildings with one to six storeys located in areas of high seismicity. Using ETABS v2018, the seismic performance prescribed by the new Algerian code RPA 2024 is compared with that of RPA 99/2003 and with several historical seismic records, including El Centro, Kobe, and Boumerdès (Dar El-Beïda station, Algeria). The results show that the seismic response of the studied structures depends strongly on building height and on the compatibility between the fundamental period and the characteristics of the response spectra. While RPA 2024 introduces more stringent requirements for low-rise buildings, certain records, particularly Kobe, lead to seismic responses that significantly exceed the corresponding code-based demands. These findings indicate that some seismic design approaches may be exposed to demand levels not fully captured by current codes. The study underscores the importance of considering severe seismic scenarios in compliance checks and highlights the need to adapt the seismic performance of existing buildings to the new regulatory framework.

1. Introduction

Algeria's position along the Africa–Eurasia plate boundary and the recurrent seismicity of the Tell Atlas—illustrated by damaging earthquakes such as El Asnam (1980) and Boumerdès have motivated successive revisions of the national seismic code, from RPA 81 to the recently implemented RPA 2024 [1–6]. The new standard clarifies performance-based objectives and introduces period-dependent soil amplification factors (S, T1–T3), which substantially reshape the design response spectrum [4–6]. These spectral modifications generally increase base-shear demands at short periods while driving mid- to long-period systems more strongly toward drift and stability control. Such changes are particularly critical for self-stable reinforced concrete (RC) moment-resisting frames—widely used in Algeria, characterized by the absence of shear walls, and therefore highly sensitive to stiffness degradation, P–Δ effects, and site-dependent spectral amplification [7–10].

*Corresponding author: a.boudina@univ-dbkm.dz
[a]orcid.org/ 0000-0003-1640-8599; [b]orcid.org/0000-0002-4615-2179; [c]orcid.org/ 0000-0003-2058-0068; [d]orcid.org/ 0000-0003-3996-2103; [e]orcid.org/ 0000-0002-2734-5709
DOI: http://dx.doi.org/10.17515/resm2025-1070ea0808rs

Previous research has examined the limitations of earlier RPA spectra with respect to recorded ground motions, the relative stringency of drift and separation criteria in RPA 99/2003 compared with Eurocode 8, and the improved lateral performance of wall–frame systems, while repeatedly highlighting the vulnerability of purely frame-type, self-stable RC structures under strong shaking [11–22]. At the mechanism level, several studies have shown that near-fault ground motions with a strong velocity pulse can produce amplified elastic and inelastic demands when the fundamental period T1 approaches the pulse period Tp, leading to elevated storey drifts, larger overturning moments, and potential activation of P–Δ sensitivity [20–25]. Canonical records such as Kobe/JMA 1995 and El Centro 1940 illustrate the combined influence of pulse proximity and spectral shape that is directly relevant to Algerian conditions [20–25]. With RPA 2024 now in force, there is a need for transparent, mechanism-focused evidence that quantifies how the updated spectrum modifies demands on self-stable frames and how these effects interact with site-tuned and near-fault ground motions in routine design contexts [24–25].

Against this background, the present study delivers the first reproducible benchmark that isolates the code-driven spectral effects introduced by RPA 2024 on self-stable Algerian RC moment-resisting frames. A uniform linear modal response-spectrum framework is employed for archetypal 1–6-storey frames, enabling controlled comparisons between RPA 2024, RPA 99/2003, and representative recorded motions [15–16]. The methodology is explicitly structured to decouple: (i) the influence of updated spectral ordinates and soil amplification parameters; (ii) the role of period elongation and stiffness redistribution; and (iii) the height-dependent sensitivity of inter-storey drift and stability indices. This separation allows the mechanisms behind observed changes in base shear, overturning, and drift to be quantified independently of record-to-record variability, moving beyond descriptive code comparison toward genuine engineering insight [15–16].

In doing so, the study fills a gap in the Algerian seismic engineering literature, which has so far lacked a controlled, reproducible benchmark focused on self-stable RC frames under the new RPA 2024 provisions [11–22]. The results are interpreted in terms of spectral shape, period–pulse alignment, and drift/stability sensitivity, and are later translated into non-prescriptive, practice-oriented screening checks and verification priorities that are explicitly distinguished from the mandatory RPA requirements [24–25]. This dual emphasis—on mechanism-based understanding and carefully framed practical implications—aims to support both code development discussions and day-to-day design decisions for existing and new RC frame structures in Algeria.

2. Studied Structures and Modeling Parameters

2.1. Structure Typology

This study considers self-stable reinforced concrete (RC) moment-resisting frame structures with regular spans of 4 m in the XX direction and 5 m in the YY direction (see Figure 1A). The buildings are located in a high-seismicity region—Zone III under RPA 99/2003 and Zone VI under RPA 2024 [5, 6] Heights vary across the archetypes (Figure 1B), and Table 1 summarizes the dimensions of load-bearing elements. All structures are modeled with fixed bases and rigid diaphragms (chosen due to the absence of large openings and lx/ly < 25%), which transfer in-plane forces to the lateral system [6]. No RC shear walls are included; lateral resistance is provided exclusively by the moment-resisting frames. Architectural infills are excluded from the analytical stiffness model (non-structural).

2.2. Materials and Loads

The concrete used in all buildings has a density of 25 kN/m^3 and a characteristic compressive strength is fck=25 MPa. Its modulus of elasticity is taken as Ec = 11000×(fck)$^{(1/3)}$), with Poisson's ratio ν=0.2, while the reinforcing steel has a density of 77 kN/m^3, a modulus Es=200 GPa, and Poisson's ratio ν=0.30. The gravitational loads include a dead load G=5 kN/m^2 and a live load Q=1.5 kN/m^2, in accordance with DTR BC 22 requirements [26]. However, the structural performance analysis focuses primarily on the effects of lateral loads, particularly those of seismic origin. For the calculation of seismic weight, the load considered is WG + 0.2WQ according to RPA99/v2003 [5], and WG + 0.3WQ according to RPA 2024 regulations [6]. Consequently, the evolution of these

standards leads to an approximate 10% increase in the proportion of live load included in the seismic weight under RPA 2024 compared with RPA 99/2003.

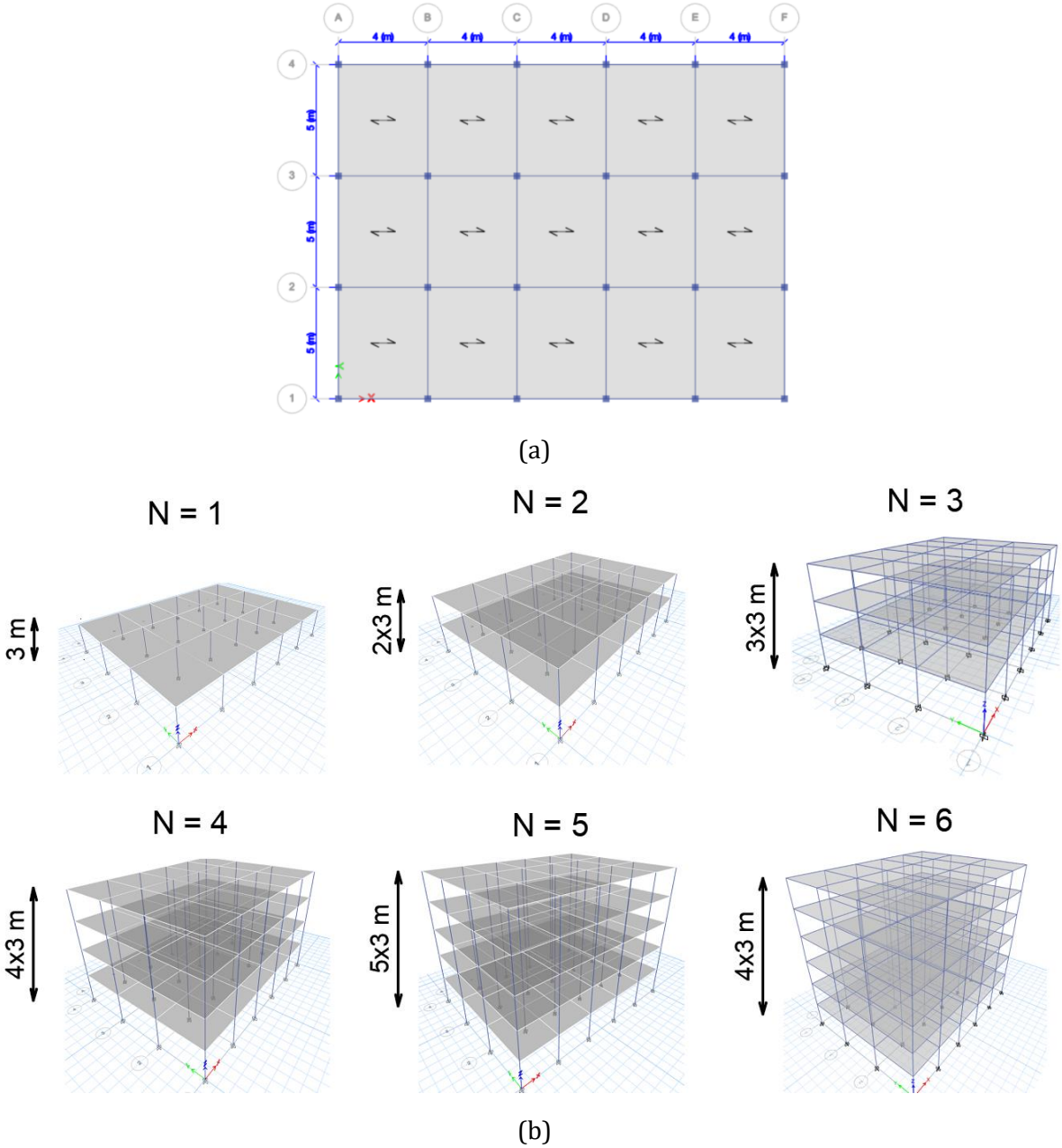

Fig. 1. Archetype self-stable RC frame building: (A) plan layout; (B) elevation configurations

Table 1. Specific properties of the reinforced concrete elements (cm)

	Section of Column (cm×cm)					
Building configurations	N=1	N=2	N=3	N=4	N=5	N=6
Storey : 1	30×30	30×30	35×35	35×35	40×40	40×40
Storey : 2		30×30	30×30	35×35	35×35	40×40
Storey : 3			30×30	30×30	35×35	35×35
Storey : 4				30×30	30×30	35×35
Storey : 5					30×30	30×30
Storey : 6						30×30

2.3. Seismic Parameters

Seismic action is represented by a horizontal 6%-damped response spectrum in both codes. The RPA 99/2003 spectrum is specified by Eqs. (1a–d), and RPA 2024 by Eqs. (2a–d).

$$\frac{S_a}{g}=\begin{cases}1.25A\left(1+\frac{T}{T_1}\left(2.5\eta\frac{Q}{R}-1\right)\right) & 0\le T\le T_1 \quad (1a)\\ 1.25A\cdot(2.5\eta)\left(\frac{Q}{R}\right) & T_1\le T\le T_2 \quad (1b)\\ 1.25A\cdot(2.5\eta)\left(\frac{Q}{R}\right)\left(\frac{T_2}{T}\right)^{2/3} & T_2\le T\le 3\ s \quad (1c)\\ 1.25A\cdot(2.5\eta)\left(\frac{Q}{R}\right)\left(\frac{T_2}{3}\right)^{2/3}\left(\frac{3}{T}\right)^{5/3} & T>3\ s \quad (1d)\end{cases}$$

where S_a/g is an acceleration response spectrum, A is the seismic acceleration coefficient (A=0.25), T is the fundamental period (sec), T_1 and T_2 are characteristic periods of the spectrum that depend on soil class (T_1=0.15 s, T_2=0.30 s), η is a damping correction factor ($\eta=\sqrt{(7/((2+\xi)))}\ge 0.7$) where ξ is a viscous damping ratio in % (ξ=6), Q is the quality factor (Q=1) and R is behavior factor (R=5).

$$\frac{S_{ad}}{g}=\begin{cases}A.I.S\left(\frac{2}{3}+\frac{T}{T_1}\left(2.5\frac{Q}{R}-\frac{2}{3}\right)\right) & 0\le T<T_1 \quad (2a)\\ A.I.S\left(2.5\frac{Q}{R}\right) & T_1\le T<T_2 \quad (2b)\\ A.I.S\left(2.5\frac{Q}{R}\right)\left(\frac{T_2}{T}\right) & T_2\le T<T_3 \quad (2c)\\ A.I.S\left(2.5\frac{Q}{R}\right)\left(\frac{T_2.T_3}{T^2}\right) & T_3\le T<4\ s \quad (2d)\end{cases}$$

where S_{ad}/g is an acceleration response spectrum, A is the seismic acceleration coefficient (A=0.30), T is fundamental period (sec), I is the building importance coefficient (I=1), S is the soil parameter (S=1), T_1, T_2 and T_3 are characteristic periods of the spectrum depend on soil class (T_1=0.10 s, T_2=0.40 s, T_3=2.0 s), Q is the quality factor (Q=1.2 or Q=1 depending on the case) and R is behavior factor (R=5.5), for more information see appendix A .

In the new RPA 2024 regulation [6], several changes have been introduced to enhance seismic safety (Table 2). The seismic acceleration coefficient A is increased from 0.25 to 0.30, reflecting stricter seismic resistance requirements, and the behavior factor R is raised from 5.0 to 5.5 for standard designs to better represent improved ductility capacity.

Table 2. Parameters applied to buildings as specified by the RPA99/v2003 and 2024 code

Seismic parameters	Symbol	RPA99/v2003	RPA2024	
		Value for all storey	1 storey	2 to 6 storeys
Acceleration coefficient of the zone	A	0.25	0.30	0.30
Quality factor	Q	1.00	1.20	1.00
Behaviour factor	R	5.00	5.50	5.50
Characteristic period of S_1 soil (sec)	T_1	0.15	0.10	0.10
Characteristic period of S_1 soil (sec)	T_2	0.30	0.40	0.40
Characteristic period of S_1 soil (sec)	T_3	-	2.00	2.00
Damping ratio (%)	ξ	6	6	6
Damping correction factor	η	0.9354	-	-

The quality factor (Q) has also been modified for certain building types to better align with their structural characteristics and intended use. For dynamic modelling, the characteristic period intervals (T1, T2) are expanded and a new period T3=2.0 s is introduced, allowing the spectrum to

better represent flexible structures. As a result, the RPA 2024 response spectrum is generally broader and higher than in RPA 99/2003, leading to more demanding seismic design criteria.

In this study, the calculation of the total seismic force or base shear (V) at the building's base is determined in both orthogonal horizontal directions (eq.3). This is performed by applying formulas 3 and 5, provided for RPA99/2003 and RPA2024 [5, 6], respectively. The various parameters associated with this static seismic force are presented in Table 3.

$$V = \frac{A\,D\,Q}{R}\ x\ W \tag{3}$$

where A, Q, and R are coefficients fixed in Table 2, and D is the dynamic amplification coefficient is given by the formula (eq.4) [6]:

$$D = \begin{cases} (2.5\eta) & 0 \le T \le T_2 \\ (2.5\eta)\left(\frac{T_2}{T}\right)^{2/3} & T_2 \le T \le 3.0\ s \\ (2.5\eta)\left(\frac{T_2}{3}\right)^{2/3}\left(\frac{3}{T}\right)^{5/3} & T > 3\ s \end{cases} \tag{4}$$

$$V = \lambda \times \frac{S_{ad}}{g}(T_0) \times W \tag{5}$$

where λ, $S_{ad}/g(T_0)$ and W are parameters fixed in Table 3.

According to Table 3, RPA 2024 differs from RPA 99/2003 by explicitly accounting for live load, introducing a correction coefficient related to the fundamental period, and basing the static force directly on the design spectrum. This leads to a more integrated representation of dynamic behaviour while generally imposing stricter seismic safety requirements.

Figure 2 displays the accelerograms of the 1940 El Centro, Kobe, and Boumerdès 2003 (Dar El-Beida station) earthquakes. The recordings obtained during these seismic events enabled the extraction of the corresponding response spectra, presented in Figure 3. Whether derived from design codes or real seismic data, the use of such spectra is essential for the seismic analysis of buildings, especially for self-stable frame structures.

Table 3. Parameters and assumed values for base shear

Letters	Description	RPA 99/2003	RPA 2024
A	Acceleration coefficient	0.25	0.30
R	Behaviour factor	5.00	5.50
Q	Quality factor	1.00	1.20 or 1.00
D	Dynamic amplification factor as a function of period and damping.	Formula (eq. 4)	-
W	Total seismic weight of the building as a function of permanent loads and live loads	$W_{Gi} + 0.2W_{Qi}$	$W_{Gi}+0.3W_{Qi}$
λ	Correction coefficient	-	0.85 if $T_0 \le 2T_2$ 1 otherwise
$S_{ad}/g(T_0)$	Ordinate of the calculation spectrum for period T_0	-	Spectrum formula (eq. 2)
T_0	Fundamental period of vibration of the building	Min $\{C_T \times h^{3/4}$; $0.09h_n/\sqrt{D_{(x,y)}}\}$	$C_T \times h^{3/4}$

The response spectra of the RPA99/v2003 and RPA2024 codes display a broad plateau followed by a consistent decrease in acceleration, whereas spectra derived from real earthquakes (El Centro, Kobe, Boumerdès) feature distinct acceleration peaks at specific periods, reflecting the inherent variability of seismic demands. Code-based spectra cover a wider period range but tend to smooth out local peculiarities present in real records. For very short periods, differences reflect the change

in T_1 from 0.15 s (RPA 99/2003) to 0.10 s (RPA 2024), which can alter short-period ordinates and affect low-rise, stiff systems.

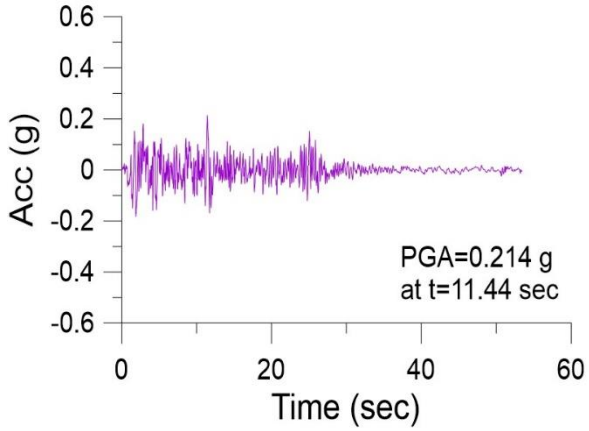

(a) El-Centro E-W

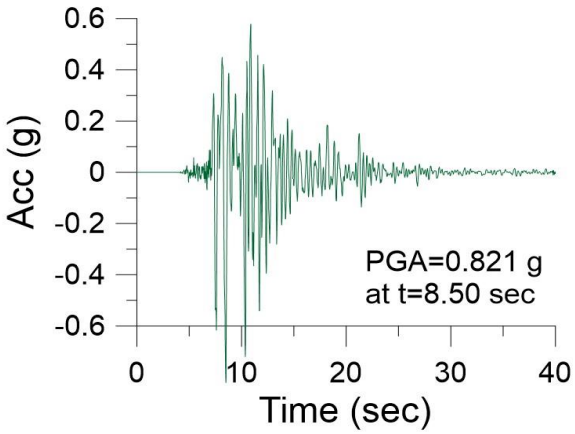

(b) Kobe (KJM) E-W

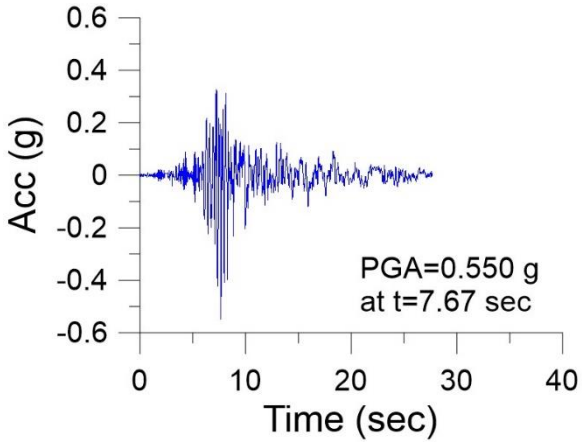

(c) Dar El-Beida E-W

Fig. 2. Horizontal acceleration time histories of the selected ground motions (El Centro 1940, Kobe/JMA 1995, Boumerdès 2003, and Dar El-Beïda 2003)

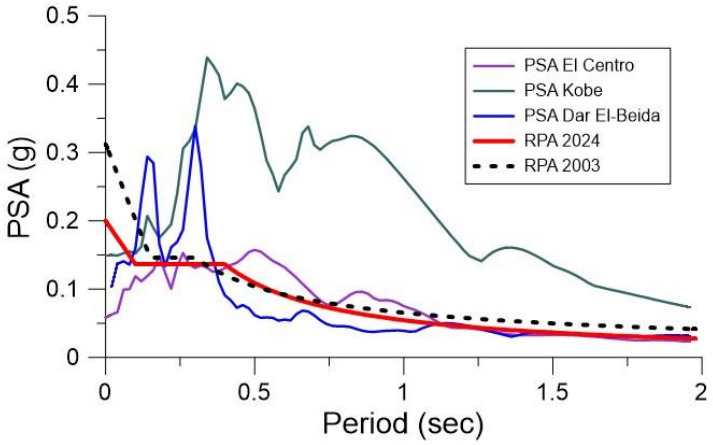

Fig. 3. 6%-damped elastic response spectra for the code spectra (RPA 99/2003 and RPA 2024) and the selected recorded ground motions

To verify modelling robustness, we performed compact quantitative checks**.** The storey-stability index θ (Eq. 7) was evaluated for all storeys, directions, spectra, and codes; the envelope is θ_{max} = 0.098 (RPA 2024, N = 6) and 0.089 (RPA 99/2003). Because $\theta_{max} < 0.10$, explicit P–Δ amplification was safely neglected. A mesh-refinement trial (doubling member segmentation and increasing

diaphragm constraints) produced $\Delta T_1/T_1 \leq 2\%$, roof-IDR ≤ 3%, V/W ≤ 3%, indicating mesh-independent results.

Modal sufficiency was confirmed by ≥ 95% cumulative translational mass participation in each direction (typically 6–10 modes for N = 1–3; 10–16 modes for N = 4–6); adding two modes changed roof IDR and V/W by ≤ 1%. A ± 10% perturbation of T_1 yielded V/W ≤ 8% and roof IDR ≤ 12%; comparative conclusions (code-to-code and record hierarchy) were unaffected. Floors were modelled as rigid diaphragms; a semi-rigid trial changed IDR by ≤ 3%. Infills were excluded to isolate frame behaviour; their implications for stiffness/irregularity are acknowledged in the Results.

2.4 Quantitative Checks and Sensitivity Summary

To ensure that the comparative results reported in Section 3 are not artefacts of numerical modelling assumptions, a series of quantitative verification and sensitivity checks was performed. These checks are intended to substantiate model reliability rather than to provide additional results; a constant damping ratio ξ = 6% is adopted throughout, consistent with RPA 2024. Table 4 summarizes the verification procedures and associated envelope metrics, while Table 5 reports the maximum storey-stability index θmax by height and code.

The storey-stability index θ, evaluated from Eq. (7) at every storey, direction, spectrum and code, attains envelope values of θmax = 0.098 for RPA 2024 (N = 6) and 0.089 for RPA 99/2003, i.e. θ < 0.10 in all configurations. This confirms that explicit P–Δ amplification is not required in the elastic analyses and provides a consistent stability baseline for the comparisons. Mesh refinement—implemented by doubling member segmentation and refining diaphragm constraints—produces changes of ΔT1/T1 ≤ 2 %, roof inter-storey drift ratio (IDR) ≤ 3 %, and base-shear ratio V/W ≤ 3 %, indicating mesh-independent behavior for the reported response metrics.

Modal sufficiency is ensured by retaining enough modes to reach at least 95 % cumulative translational mass in each principal direction (typically 6–10 modes for N = 1–3 and 10–16 modes for N = 4–6). Adding two extra modes modifies roof IDR and V/W by ≤ 1 %, showing that modal truncation has a negligible influence on the key response quantities. Finally, a ±10 % perturbation of T1 (representing period uncertainty) leads to variations of V/W ≤ 8 % and roof IDR ≤ 12 %, without altering the qualitative trends between codes, heights or spectra. Overall, Tables 4 and 5 indicate that base shear and overturning are essentially insensitive to the tested modelling variations, whereas drifts and θ exhibit only modest sensitivity, supporting the robustness of the conclusions drawn in Section 3.

Table 4. Quantitative checks and sensitivity summary (envelopes over XX/YY, all spectra, both codes)

Verification item	Procedure	Metric reported	Result (envelope)	Interpretation
Storey-stability index θmax	Evaluate Eq. (7) at every storey	θ_{max}	0.098 (RPA 2024, (N=6)); 0.089 (RPA 99/2003); all (θ<0.10)	Explicit P– Δ amplification not required
Mesh-refinement test	Double member segmentation; denser diaphragm constraints	Δ T_1/T_1), Δ roof IDR, Δ (V/W)	≤2%, ≤3%, ≤3%	Mesh-independent for reported metrics
Modal sufficiency	Retain modes to ≥95% mass; add +2 modes	Cumulative mass; Δ roof IDR, (V/W)	Achieved; changes ≤1%	Modal truncation adequate
(T_1) uncertainty	Perturb (T_1 ±10%)	Δ(V/W); Δroof IDR	≤8%; ≤12%	Conclusions robust to (T_1) shifts

Table 4 summarizes these quantitative checks and sensitivity analyses, presenting the verification procedure, metrics, results, and interpretations of stability index, mesh refinement, modal sufficiency, and period uncertainty. Table 5 breaks down θmax values by building height and code

(maximum values over directions and spectra), showing a gradual increase with the number of storeys but values remaining below threshold limits, thus affirming structural stability across configurations.

Table 5. θmax by height and code (max over directions and spectra; see Table 7 for per-direction values)

(N)	θmax RPA 99/2003	θmax RPA 2024
1	0.022	0.019
2	0.025	0.027
3	0.035	0.037
4	0.051	0.058
5	0.079	0.086
6	0.089	0.098

3. Results and Discussion

Two mechanisms govern the observed trends. For mid-rise frames (N≥4), the reduction in base shear under RPA 2024 primarily reflects longer effective periods T_1 and lower spectral ordinates at those periods, so drift and the storey-stability index θ become the critical checks rather than force. When T_1 aligns with a near-fault velocity-pulse period Tp, exemplified by the Kobe record, inter-storey drift and θ both increase due to directivity-induced pulse effects under RPA 2024 micro zonation and period-dependent amplification.

The results are interpreted in terms of two mechanisms: increased drift and θ under pulse-like records when $T_1 \approx Tp$ and reduced base shear for mid-rise frames under the new spectral shape at longer periods. In practice, engineers should prioritize drift verification and θ screening when T_1 is close to Tp and include pulse-like motions in record selection when T_1 lies between 0.5 and 1.0s.

Rather than introducing new algorithms, this study provides a reproducible benchmark that compares RPA 2024 with RPA 99/2003 and representative records, isolates how the spectral updates redistribute elastic demand, and translates these shifts into concise, actionable checks for designers and code developers.

3.1 Lateral Displacements

Figure 4 presents maximum storey displacements as a function of spectrum and building height. Displacements increase with height, reflecting first-mode dominance. The near-fault Kobe record governs displacements across all heights because of velocity-pulse amplification when T1≈Tp, whereas El Centro remains close to the code spectra for mid- and high-rise frames and Boumerdès is severe mainly for low-rise cases. Directional differences between XX and YY are small, which confirms the regularity of the archetype buildings.

Demand assessment uses spectral acceleration at the first-mode period Sa (T1, 6%), normalized drift IDR = Δ/h, and storey stability index θ, with checks for serviceability drift and P–Δ stability performed per Eurocode 8 [25]. Practical mitigation strategies include supplemental damping or base isolation to reduce IDR and base shear V/W, detuning T1 outside the pulse bandwidth, and capacity design of lower storeys; iterations follow Eurocode 8 validation criteria [27].

Maximum elastic storey-displacement profiles for archetype frames (N = 1–6) under code-based and recorded spectra. Results highlight the relative displacement demand across building heights without interpretation in the caption. As shown in Fig. 4, Kobe governs the displacement demands, while El Centro and Boumerdès remain broadly consistent with the code spectra across the investigated heights. This behavior follows the relation $Sd(T) \propto (T/2\pi)^2 \cdot Sa(T)$: taller frames under RPA 2024 have larger T_1 with lower $Sa(T_1)$ on the long-period branch, reducing elastic forces so that drift and θ govern for N≥4 .

Northern Algerian fault systems can generate directivity pulses at short distances, so pulse-like records are critical for verifying the seismic performance of self-stable RC frames. Kobe is used as a near-fault proxy: Tp aligning with T_1 leads to concentrated inter-storey drift and elevated θ even

when base shear is not controlling. This supports routine use of pulse-enriched records in Algerian practice and guides future RPA calibration.

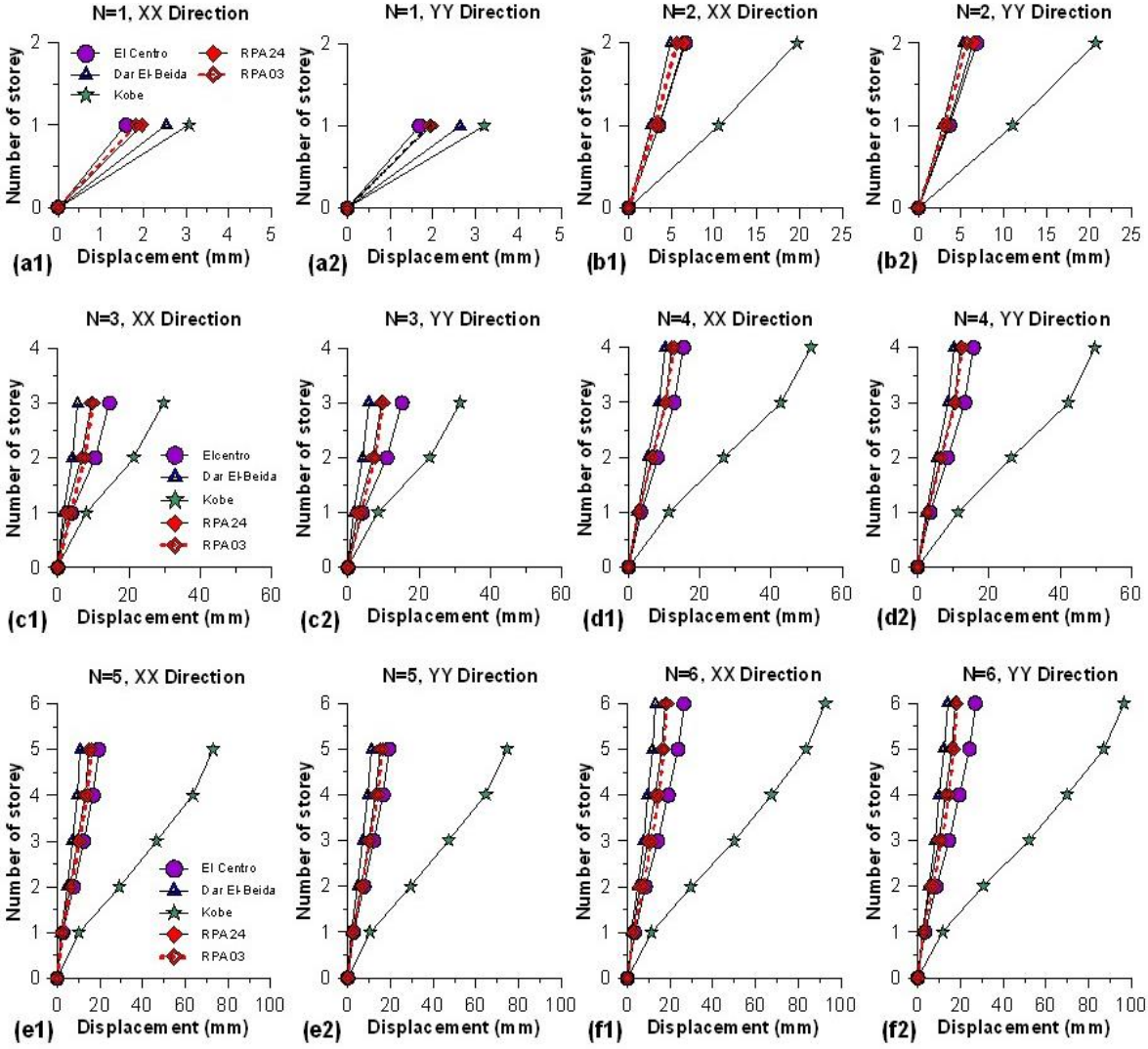

Fig. 4. Maximum elastic storey-displacement profiles in directions XX and YY for the archetype frames (N = 1–6) under code-based and recorded spectra

Table 6. Comparison of maximum elastic displacements between the two RPA codes (mm)

N	RPA2024 XX	RPA99/2003 XX	variation XX (%)	RPA2024 YY	RPA99/2003 YY	variation YY (%)
1	1.96	1.84	+6.74	1.95	1.92	+1.40
2	6.48	5.98	+8.26	6.45	6.23	+3.38
3	9.31	9.27	+0.43	9.37	9.63	-2.69
4	12.28	12.72	-3.46	12.23	12.58	-2.78
5	14.87	16.73	-11.14	15.03	17.34	-13.31
6	17.65	20.82	-15.26	17.87	21.55	-17.10

El Centro and RPA spectra cluster for mid-/high-rise frames, with El Centro sometimes exceeding RPA demands at larger N [28]. Boumerdès exerts greater influence at short periods but fades with height, reinforcing the need to complement design spectra with record-based displacement checks. Across all heights, Kobe remains the most demanding motion, with El Centro and the RPA spectra clustering at intermediate levels and Boumerdès dominating only low-rise cases (N ≤ 2–3), as shown in Fig. 4. Table 6 summarizes that RPA 2024 yields slightly higher displacements for N=1–2, while RPA 99/2003 dominates from N≥3, affirming the regulatory effect on displacement-based design.

The regulatory framework notably influences displacement estimates and consequent design choices, especially for medium- and high-rise buildings. Compared to RPA 99/2003, RPA 2024 introduces a height-dependent, non-uniform demand shift due to its updated hazard basis and period-dependent amplification. This adjustment better suits typical Algerian building typologies, though its effects on safety margins and costs require case-by-case evaluation. To ensure consistency across tables, percentage differences are computed as:

$$\text{Variation (\%)} = \frac{X_{\text{RPA 2024}} - X_{\text{RPA 99/2003}}}{X_{\text{RPA 99/2003}}} \times 100. \quad (6)$$

Table 7 compares inter-storey drift by height (N) and direction (XX, YY) against each code's limits. RPA 99/2003 limits the storey drift ratio to 1.0% of storey height, while RPA 2024 allows up to 1.5%. Although all computed drifts meet these limits, caution is advised as Ozmen et al. [29] show that soft-storey irregularities can concentrate drift and cause damage despite overall compliance.

As summarized in Tables 4 and 5, θ remains below 0.10 in all cases, with only modest sensitivity of θ and inter-storey drift to mesh refinement, modal truncation, and ±10% variations in T_1, thereby justifying the neglect of explicit P–Δ effects in the elastic analyses [5, 6].

$$\theta = \frac{P_{tot} \times \Delta_k}{V_{tot} \times h} \leq 0.10 \quad (7)$$

where P_{tot} is total gravity load at and above the storey being considered, V_{tot} is total seismic shear force at that storey, Δ_k is design value of the inter-storey drift, and h is height of the storey.

Table 7. The max inter-storey displacements (cm) and the max P-Δ condition between the two RPA codes

	RPA99/2003						RPA2024					
N	Δ_k XX	Δ_k YY	Allow-able	θ_xx	θ_yy	Allow-able	Δ_k XX	Δ_k YY	Allow-able	θ_xx	θ_yy	Allow-able
1	0.92	0.96	3.00	0.021	0.022	0.10	0.90	0.89	4.50	0.019	0.019	0.10
2	1.59	1.67	3.00	0.024	0.025	0.10	1.92	1.93	4.50	0.026	0.027	0.10
3	2.09	2.17	3.00	0.034	0.035	0.10	2.32	2.34	4.50	0.037	0.037	0.10
4	1.94	1.96	3.00	0.051	0.051	0.10	2.08	2.10	4.50	0.058	0.058	0.10
5	2.18	2.25	3.00	0.077	0.079	0.10	2.16	2.19	4.50	0.086	0.086	0.10
6	2.29	2.36	3.00	0.088	0.089	0.10	2.14	2.17	4.50	0.098	0.098	0.10

As a quantitative check, the maximum envelope value θmax across all cases is 0.098 < 0.10 for RPA 2024 (N=6), with the corresponding maximum under RPA 99/2003 being 0.089. This confirms neglecting explicit P–Δ amplification in elastic analyses. This holds for all building heights and both principal directions.

3.2 Base Shear Forces

The hierarchy of base-shear demand follows the spectral acceleration at the first-mode period Sa(T1,6%). Under RPA 2024, longer T1 values and lower spectral ordinates beyond the corner period reduce V/W for mid- and high-rise frames. Near-fault motions (e.g., Kobe) offset this by concentrating spectral energy near a pulse period T_p close to T_1, sustaining force and drift demand when $T_1 \approx T_p$. Kobe consistently produces the largest base shear, confirming the severity of near-fault pulse-like scenarios compared to local code spectra and regional records [3, 4]. Elevated demand at taller heights aligns with higher Sa(T_1) near the pulse in the Kobe spectrum (Figure 5).

Comparisons between normalized forces and Sa(T1,6%) identify pulse–period resonance for the Kobe record. Drift limits from Eurocode 8, second-order stability checks based on θ, and torsional sensitivity checks are used to establish safety margins that are independent of absolute base shear [27]. Mitigation strategies include adding supplemental damping or isolation, retuning the structure to shift T1 away from the pulse band, and applying capacity design in the lower storeys. Performance is then verified iteratively against FEMA-445 and Eurocode 8 criteria [15, 27].

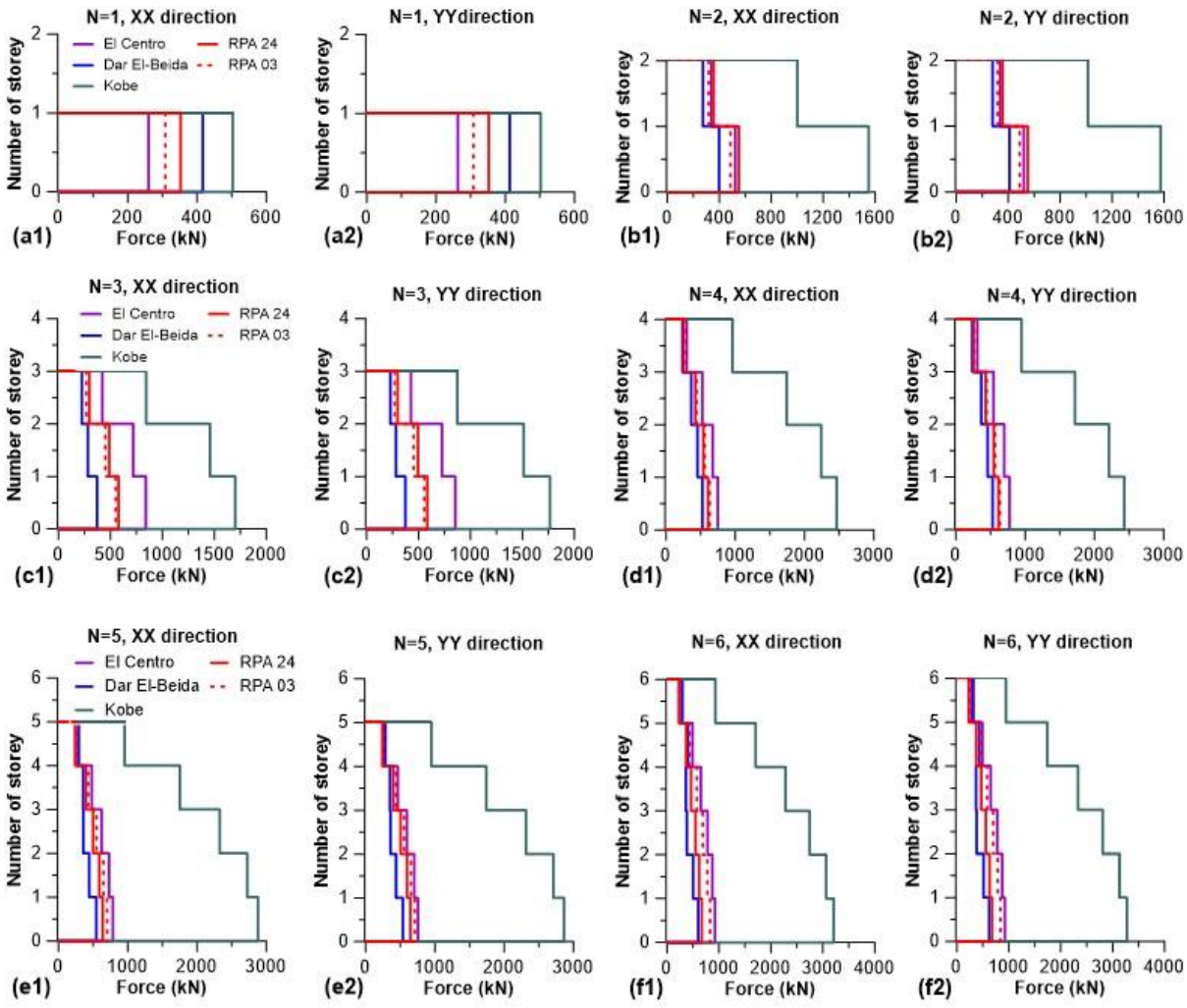

Fig. 5. Storey-shear distributions and total base shear V in directions XX and YY for the archetype frames (N = 1–6)

Base-shear distribution profiles for archetype frames (N = 1–6) across spectra and directions. The figure presents envelope values used for comparative assessment. The El Centro spectrum shows an intermediate base shear demand: at taller heights (e.g., N=6), it surpasses Dar El-Beïda and both RPA spectra (Fig. 5; Table 9). This results from stronger spectral ordinates in the mid-period range, emphasizing the importance of accurately estimating the fundamental period T_1, considering structural properties like span length and column stiffness rather than height alone [30]. Following Ivanov and Velchev [31], the choice between recorded and code spectra significantly affects force predictions. Dar El-Beïda mainly impacts short-period, low-rise frames but its effect diminishes at greater heights due to spectral ordinate decay. Consistent with Pashova et al. [32], verifying code spectra against representative recorded motions is essential to uncover vulnerabilities not evident in a single normative spectrum.

All analyses comply with FEMA-445 [15] and Eurocode 8 guidelines [27], which advise against relying solely on one design spectrum and recommend incorporating extreme and actual recorded ground motions to ensure seismic resilience. Base shear results under RPA 2024 and RPA 99/2003 display divergent trends with height: RPA 2024 shows moderately increased base shear for short periods (N = 1–3) due to elevated short-period spectral ordinates (see Table 9), while for taller structures (beyond N ≈ 4), RPA 99/2003 prevails. This change stems from longer effective fundamental periods and lowered spectral ordinates in RPA 2024's long-period range, leading to reduced $Sa(T_1)$ and V/W ratios for tall frames, while drift and the storey stability index θ remain dominant factors.

Table 8 provides conservative screening multipliers to flag cases needing refined analyses, such as expanded record sets or nonlinear evaluations, supplementing but not replacing RPA code compliance. These factors of screening are indicative tools and do not substitute for RPA regulatory provisions.

Table 8. Practitioner screening checks for self-stable RC frames (conservative; not a replacement for RPA provisions)

Check	Trigger / Condition	Screening multiplier	Use / Action
Drift (far-field baseline)	Typical design sets without near-fault indicators	IDR_screen = 1.15 × IDR_RPA2024	If screened IDR exceeds SLS/ULS limits, expand record set and/or run targeted nonlinear checks.
Drift (near-fault trigger)	$T_1 \in [0.5, 1.0]$ s or plausible fault proximity	IDR_NF = 1.50 × IDR_RPA2024	Include pulse-like records; consider damping/isolators; verify local detailing and capacity design.
Base-shear envelope (N ≥ 4)	Mid-/high-rise frames	V_screen = 1.20 × V_RPA2024	Force envelope for collectors, joints, and anchors; confirm with modal combinations where critical.
Early-warning stability	θ ≥ 0.08 (code limit θ < 0.10)	θ_screen = 0.08 (trigger)	Treat as P–Δ-sensitive: check second-order effects; adjust stiffness/stability details as needed.

Table 9. Comparison of base shear forces between the two RPA codes (kN)

N	RPA 2024 XX	RPA99/ 2003 XX	variation XX (%)	RPA 2024 YY	RPA99/ 2003 YY	variation YY (%)
1	352.44	308.41	+14.28	352.44	308.41	+14.28
2	549.41	485.10	+13.26	550.04	488.08	+12.69
3	579.06	559.80	+3.44	585.42	563.85	+3.82
4	604.48	629.16	-3.92	613.48	636.06	-3.55
5	640.21	703.36	-8.98	648.54	710.21	-8.68
6	669.45	763.36	-12.30	679.36	772.19	-12.02

3.3 Overturning Moments

Overturning demand results from first-mode lateral forces acting with their lever arms along the building height. This leads to overturning moments following the displacement spectrum Sd(T) at the fundamental period T_1, increasing as forces concentrate near the roof. Near-fault pulse-like earthquakes such as Kobe increase Sa(T1, 6%) when T1 is close to the pulse period Tp which amplifies both base shear and overturning effects. This is observed in elevated normalized overturning indices Movt/(WH) and greater roof rotations ϕroof. Figure 6 illustrates that Kobe and Dar El-Beïda motions produce larger overturning moments than El Centro in both principal directions and associated codes. For example, at height N=1 under RPA 2024, Kobe's moment reaches 1509.7 kN·m compared to El Centro's 1057.3 kN·m (≈ +39%), with Dar El-Beïda also showing significantly higher values (≈1248 kN·m). These differences highlight the necessity to consider record-to-record variability and near-fault effects for realistic seismic loss and design predictions [33, 34].

The increased overturning for Kobe and Dar El-Beïda relates to directivity and pulse characteristics aligned with T_1. This is supported by (i) comparing Sa(T_1, 6%) across spectra, (ii) tracking the normalized overturning index Movt/(WH), and (iii) monitoring roof rotation ϕ_roof together with

Eurocode 8 [27] drift limits and P–Δ stability checks. Foundation bearing or uplift verifications corroborate greater overturning demands in near-pulse scenarios.

At short periods (N = 1–3), RPA 2024 yields higher overturning moments than RPA 99/2003, aligned with strengthened short-period spectral ordinates and greater static demands [35]. Beyond N ≈ 4, RPA 99/2003 governs, as longer effective periods and lower spectral ordinates in RPA 2024's long-period branch reduce Sa(T_1) and dynamic overturning in taller buildings [27]. Near-fault records like Kobe and Dar El-Beïda intensify overturning across heights due to spectral energy concentration and pulse effects [33, 34]. Accordingly, capacity design in base and lower stories is critical for N ≤ 3 under RPA 2024, while for N ≥ 4, drift, stability (θ), and foundation rocking/uplift govern the design checks [15, 27, 36].

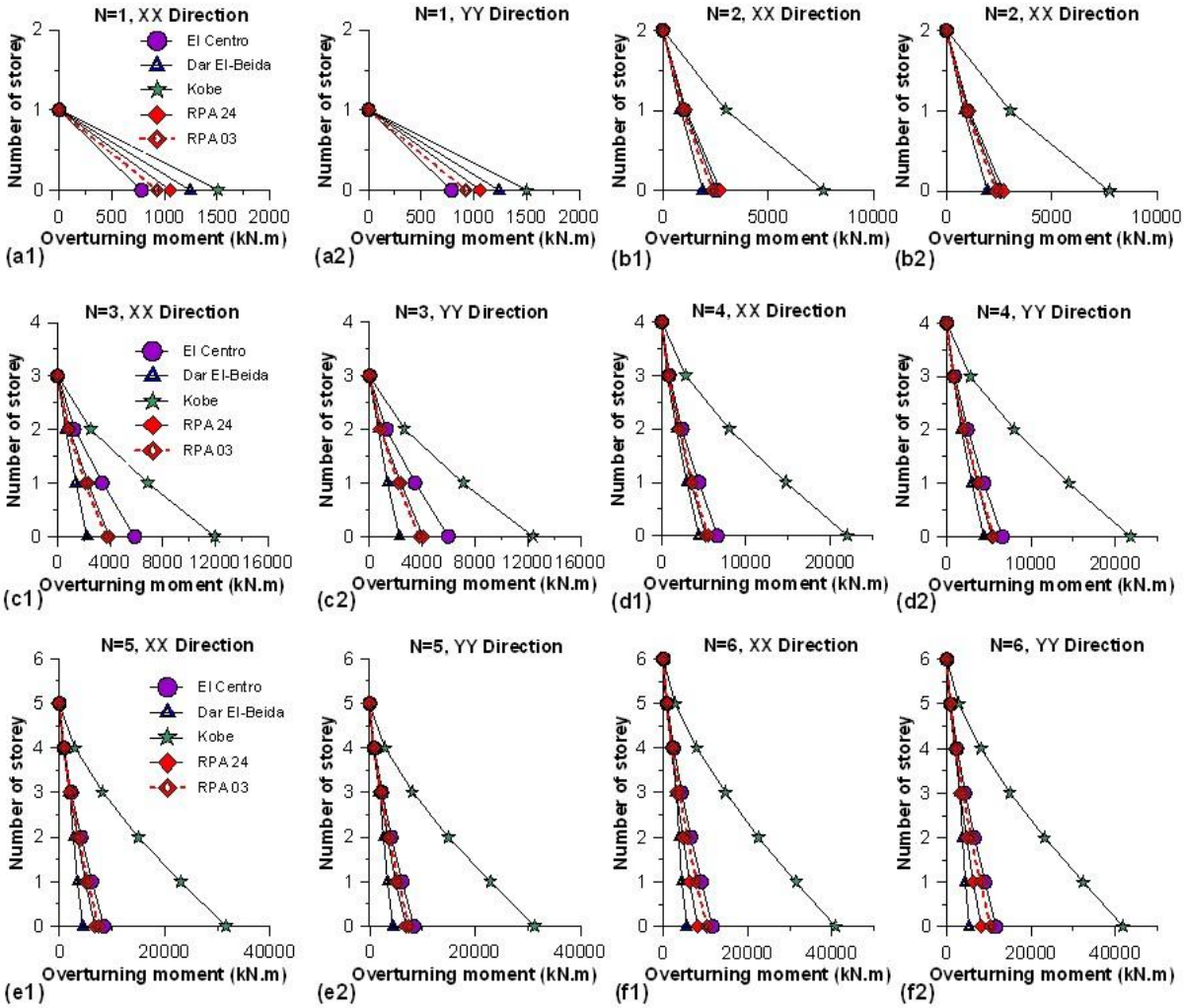

Fig. 6. Overturning-moment distributions and base overturning moments M0 in directions XX and YY for the archetype frames (N = 1–6)

Table 10. Comparison of overturning moments between the two RPA codes (kN.m)

N	RPA 2024 XX	RPA99/ 2003 XX	variation XX (%)	RPA 2024 YY	RPA99/ 2003 YY	variation YY (%)
1	1057.33	925.24	+14.28	1057.33	925.24	+14.28
2	2696.77	2371.23	+13.73	2698.35	2384.82	+13.15
3	3993.46	3829.27	+4.29	4038.56	3858.06	+4.68
4	5277.18	5488.56	-3.85	5353.00	5544.34	-3.45
5	6703.64	7364.01	-8.97	6799.46	7442.15	-8.64
6	8113.82	9392.22	-13.61	8246.93	9502.42	-13.21

Table 10 summarizes base overturning moments at the first storey. For low- to mid-rise buildings (N = 1–3), RPA 2024 yields moments 4–14% higher than RPA 99/2003 (depending on direction), reflecting tighter lower-storey demands in the updated code. From N = 4 onwards, a reversal in this trend becomes apparent: values derived from RPA2024 become lower than those from the earlier code, with reductions of around -3% at the fourth storey, increasing as the building height grows, surpassing -14% for the tallest structures. Such an adjustment confirms the intention not to demand excessively high uniformity in moment requirements for tall buildings, while maintaining stringent demands for lower-rise structures.

3.4 Ratio of Equivalent Static Force to Modal Spectral Force

Tables 11 and 12 compare the dynamic characteristics and seismic forces for buildings of varying height under RPA 99/2003 and RPA 2024. The fundamental period T0—both empirical and ETABS—rises with height, reflecting greater flexibility. Under RPA 99/2003 (Table 11), empirical periods are systematically shorter than the ETABS values, indicating a conservative bias. In contrast, RPA 2024 (Table 12) adopts longer empirical periods that align more closely with the modelled results, offering a more realistic representation of structural flexibility.

Table 11. Fundamental period of the building (T) and total storey shears for RPA99/2023

N	T_empirical (sec)		V_{Static} (kN) RPA99/v2003		T_Etabs (sec)		$V_{Dynamic}$ (kN) RPA99/v2003	
	T_{min_XX}	T_{min_YY}	V_{xx}	V_{yy}	T_{1_XX}	T_{1_YY}	V_{XX}	V_{YY}
1	0.060	0.070	251.51	251.51	0.218	0.217	308.41	308.41
2	0.121	0.139	512.49	512.49	0.391	0.388	485.10	488.08
3	0.181	0.209	776.89	776.89	0.524	0.519	559.80	563.85
4	0.242	0.279	1044.71	1044.71	0.671	0.661	629.16	636.06
5	0.302	0.349	1311.04	1191.16	0.791	0.779	703.36	710.21
6	0.362	0.418	1404.14	1275.74	0.924	0.909	763.36	772.19

Table 12. Fundamental period of the building (T0) and total storey shears for RPA2024

N	T_0 empirical in XX and YY (sec)	V_{Static} (kN) RPA2024		Fundamental period T_Etabs (sec)		$V_{Dynamic}$ (kN) RPA 2024	
		V_{XX}	V_{YY}	T_{1_XX}	T_{1_YY}	V_{XX}	V_{YY}
1	0.114	359.35	359.35	0.220	0.219	352.44	352.44
2	0.192	609.95	609.95	0.395	0.392	549.41	550.04
3	0.260	785.78	785.78	0.530	0.524	579.06	585.42
4	0.322	1008.38	1008.38	0.677	0.668	604.49	613.49
5	0.381	1074.70	1074.70	0.799	0.787	640.21	648.54
6	0.437	1133.49	1133.49	0.934	0.918	669.45	679.36

RPA 2024 prescribes higher static base shear forces (Vstatic) for low-rise buildings (N = 1–2), reflecting updated live-load coefficients and increased short-period spectral ordinates, whereas for mid- and high-rise frames (N ≥ 3–4) the longer effective periods and reduced long-period spectral ordinates lead to static and dynamic base shears that are comparable to or lower than those under RPA 99/2003 (Tables 11–13). In both codes, the ratio Vdynamic/Vstatic increases with height, but it peaks earlier and at higher values under RPA 99/2003, while RPA 2024 exhibits a more gradual increase, consistent with a more calibrated distribution of seismic demand across building heights.

Similarity of values across principal directions XX and YY confirms near-symmetric dynamic response and consistent modeling assumptions under both codes. Overall, these results reflect progress toward seismic design regulations better aligned with true structural behavior, achieved through improved vibration modeling and refined dynamic load modulation, balancing realistic structural flexibility and safety without excessive constraints.

Table 13 summarizes the normalized base shear ratios V/W for RPA 99/2003 and RPA 2024 as a function of building height. These ratios synthesize the intensity of static seismic forces prescribed

by each code and provide a compact representation of how design base shear evolves with height under the two spectral formulations. Figure 7 illustrates differential evolution of seismic demands by building height and applied code.

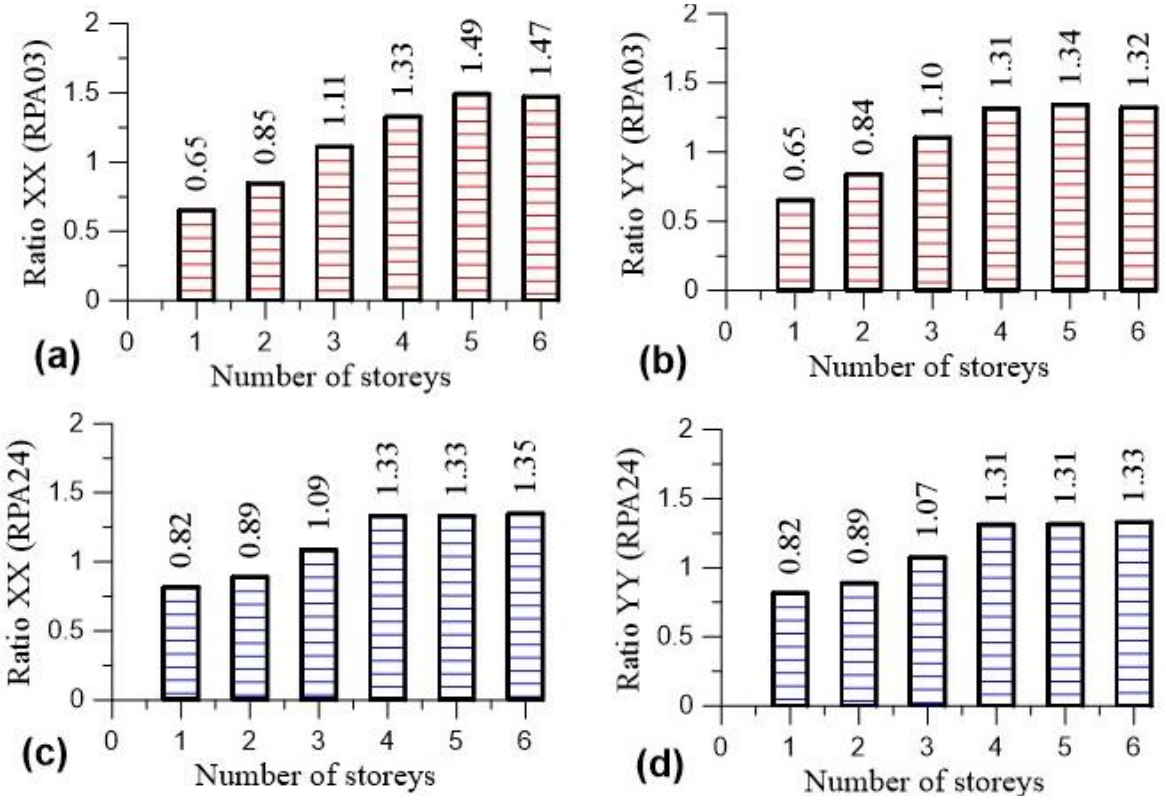

Fig. 7. Dynamic-to-static force ratios Vdynamic/Vstatic and normalised base shear V/W as a function of building height for RPA 99/2003 and RPA 2024

For low-rise buildings (N = 1 or 2), RPA 2024 specifies higher seismic design coefficients than RPA 99/2003 in both principal directions (XX and YY). This reflects an intention to strengthen the consideration of dynamic seismic effects at lower levels, consistent with Demirci et al. [37], who emphasize the importance of addressing increased seismic demands in the lower stories of multi-storey buildings to effectively manage concentration of seismic forces.

Table 13. V/W ratio for both RPA codes

	RPA99/2003					RPA 2024				
N	Weight (kN)	V_{Stat}/ W XX	V_{Stat}/ W YY	V_{dyn}/ W XX	V_{dyn}/ W YY	Weight (kN)	V_{Stat}/ W XX	V_{Stat}/ W YY	V_{dyn}/ W XX	V_{dyn}/ W YY
1	2151.00	0.12	0.12	0.14	0.14	2196.00	0.16	0.16	0.16	0.16
2	4383.00	0.12	0.12	0.11	0.11	4473.00	0.14	0.14	0.12	0.12
3	6644.25	0.12	0.12	0.08	0.08	6779.25	0.12	0.12	0.09	0.09
4	8934.75	0.12	0.12	0.07	0.07	9114.75	0.11	0.11	0.07	0.07
5	11259.00	0.12	0.11	0.06	0.06	11484.00	0.09	0.09	0.06	0.06
6	13617.00	0.10	0.09	0.06	0.06	13887.00	0.08	0.08	0.05	0.05

For medium- and high-rise buildings (N=3 to N=6), the trend reverses or moderates: from the third storey onward, the dynamic ratios under RPA2024 become slightly lower than or close to those under RPA99/v2003, signaling an alignment and optimization of code prescriptions for these categories. This moderation in demand is consistent with the observations of Lam et al. [38], who highlight the importance of precise calibration of inter-storey forces and displacements, ensuring a homogeneous structural response and avoiding unnecessary overdesign. From a directional perspective, the similarity of trends between xx and yy confirms the dynamic symmetry of the model studied and the methodological robustness of the codes. This consistent approach is also

highlighted by Şahin and Turan [39], who stress the determining influence of structural configuration and the orientation of seismic loading on the distribution of forces in various frame and shear wall building scenarios. Furthermore, the works of Merabti et al. [40] and Khelladi et al. [41] demonstrate, through parametric analysis, that the directions of seismic load application and model symmetry play a key role in the distribution of internal forces.

The normative reform introduced by RPA 2024 incorporates these changes in spectral shape and load combinations to strengthen the design of lower storeys—where dynamic demands are highest—while rationalizing force levels for taller structures. This approach aims to balance safety and economy by concentrating higher force and stability requirements in the most critical regions of self-stable RC frames, without unnecessarily increasing demand for mid- and high-rise buildings.

Across the investigated heights, Kobe and Dar El-Beïda consistently produce the largest demands due to the alignment of T_1 with their predominant velocity-pulse periods, resulting in amplified $Sa(T_1)$ and higher drift and overturning responses. For code-based spectra, RPA 2024 governs low-rise buildings (N = 1–2) through increased short-period ordinates and updated load combinations, whereas for mid- and high-rise frames (N ≥ 3–4), the longer effective periods shift the response into the reduced long-period branch of the spectrum, producing base shear and overturning values comparable to or lower than RPA 99/2003. These trends reflect the combined influence of spectral shape, period elongation, and height-dependent drift sensitivity, and they define the engineering mechanisms that govern seismic demand redistribution under the updated Algerian code.

For self-stable RC frames, our comparisons indicate that for N ≥ 4 the reduction in force demand under RPA 2024 shifts design control to drift and storey stability. Practically, engineers should (i) prioritise inter-storey drift and θ checks, (ii) cross-check the fundamental period T1 (empirical vs modal), and (iii) consider potential near-fault effects when $T1 \in [0.5,1.0]$ s or the site is within plausible fault-proximity. For routine workflows we recommend reporting ≥ 95% cumulative translational mass participation, documenting storey-wise θ, and, where near-fault exposure is credible, augmenting linear analyses with at least one pulse-like record or conditional spectrum. As conservative screening multipliers (not code substitutions), we propose $IDR_{screen}=1.15\times IDR_{RPA2024}$ for far-field cases, $IDR_{NF}=1.50\times IDR_{RPA2024}$ where near-fault effects are suspected, and $V_{screen}=1.20\times V_{RPA2024}$ for N ≥ 4 to envelope record-based forces; treat θ ≥ 0.08 as an early-warning trigger. If any screened demand exceeds limits, escalate to refined analysis (expanded record set and/or targeted nonlinear checks).

4. Conclusion

This study offers the first systematic, reproducible benchmark comparing the seismic response of self-stable Algerian RC moment-resisting frames under RPA 99/2003, RPA 2024, and representative recorded ground motions. Using a uniform linear modal response-spectrum framework for 1–6-storey archetype frames, the analysis isolates how the updated RPA 2024 spectrum redistributes elastic base shear, overturning, and inter-storey drift demands across building heights. The verification checks assembled in Section 2.4 show that the numerical results are robust with respect to mesh refinement, modal truncation, and ±10 % variations in the fundamental period, and that the storey-stability index remains below θ = 0.10 in all cases, supporting the decision to neglect explicit P–Δ amplification in the elastic analyses.

For practice, engineers designing under RPA 2024 should place particular emphasis on drift and θ checks for self-stable RC frames, especially when the fundamental period lies near the velocity-pulse range of potential near-fault motions. The results suggest that elastic force checks alone may underestimate critical response in these cases, and that targeted use of pulse-like records and simple screening criteria can help identify configurations that warrant more detailed analysis. These recommendations are formulated as non-prescriptive guidance and do not replace the mandatory RPA provisions.

The conclusions are bounded to regular, frame-only systems with the material properties, loads, and modelling assumptions adopted in this study, and to the elastic range of response. Future work should extend the benchmark to include irregular configurations, wall–frame systems, and

nonlinear analyses, and should explore a wider range of recorded motions and soil conditions. Within these limits, the findings provide a consistent reference for interpreting the implications of RPA 2024 for self-stable RC frames and can support further refinement of the code and of design practice in Algeria.

Appendix A

The calculation was carried out based on the parameters derived from the code, the values of which are presented in the following section. Tables A.1 and A.2 summarize the calculation results corresponding to each case studied.

A.1 The parameters of the RPA 99/2003 code used

A=0.25, R= 5, Q=1, ξ=6, η=0.9354, T_1=0.15, T_2=0.30, Lx= 20 m, Ly= 15 m, and C_T=0.05

Table A1. Parameters applied to buildings as specified by the RPA99/v2003 code

	RPA99/v2003					
Structure	N=1	N=2	N=3	N=4	N=5	N=6
h (m)	3	6	9	12	15	18
T_0 = Min $\{C_T \times h^{3/4}$; $0.09h/\sqrt{Lx}\}$ (sec)	0.0604	0.1207	0.1811	0.2415	0.3019	0.3622
T_0 = Min $\{C_T \times h^{3/4}$; $0.09h/\sqrt{Ly}\}$ (sec)	0.0697	0.1394	0.2091	0.2789	0.3486	0.4183
D (eq.4)	2.3385	2.3385	2.3385	2.3385	2.3289	2.0623
W= W_{Gi}+0.2W_{Qi} (kN)	2151.00	4383.00	6644.25	8934.75	11259.00	13617.00
Vx (kN)	251.51	512.49	776.89	1044.71	1311.04	1404.14
Vy (kN)	251.51	512.49	776.89	1044.71	1191.16	1275.74

A.2 The parameters of the RPA 2024 code used

A=0.30, R= 5.5, I=1.0, S=1.0, T_1=0.10, T_2=0.40, T_3=2.0 and C_T=0.05

Table A2. Parameters applied to buildings as specified by the RPA2024 code

	RPA2024					
Structure	N=1	N=2	N=3	N=4	N=5	N=6
h (m)	3	6	9	12	15	18
$T_{empirical}$= $C_T \times h^{3/4}$ (sec)	0.114	0.19**2**	0.2**60**	0.322	0.381	0.437
1.3×$T_{empirical}$	0.148	0.250	0.338	0.419	0.495	0.568
$T_{cal(ETABS)}$	0.220	0.395	0.53**0**	0.677	0.799	0.934
T_0 * (sec)	0.148	0.250	0.338	0.419	0.495	0.568
T_1 (sec)	0.10	0.10	0.10	0.10	0.10	0.10
T_2 (sec)	0.40	0.40	0.40	0.40	0.40	0.40
λ**	1.00	1.00	0.85	0.85	0.85	0.85
$S_{ad}/g(T_0)$	0.164	0.136	0.136	0.130	0.110	0.096
W= W_{Gi}+0.3W_{Qi} (kN)	2196.00	4473.00	6779.25	9114.75	11484.00	13887.00
Vx=Vy (kN)	359.35	609.95	785.78	1008.38	1074.70	1133.49

** $T_0 = T_{cal}$ if $T_{cal} < 1.3T_{empirical}$, or $T_0 = 1.3\ T_{empirical}$ if $T_{cal} \geq 1.3T_{empirical}$.*

***λ ={0.85 if T0 ≤(2 T_2) and if the building has more than 2 levels ; 1.0 otherwise}.*

References

[1] Yelles-Chaouche AK, Nour A, Maouche S. Seismicity, seismotectonics and seismic hazard in northern Algeria. In: EERI Special Earthquake Report – May 2003 Boumerdes, Algeria earthquake; 2004.

[2] Guettiche A, Guéguen P, Mimoune M. Seismic vulnerability assessment using association rule learning: application to the city of Constantine, Algeria. Natural Hazards. 2017;86(3):1223–1245. https://doi.org/10.1007/s11069-016-2739-5

[3] Taleb R. Règles Parasismiques Algériennes RPA 99 - Version 2003 pour les Structures de Bâtiments en Béton Armé: Interprétations et Propositions. Journal of Materials and Engineering Structures. 2017;4:139–154. https://revue.ummto.dz/index.php/JMES/article/view/1567/pdf

[4] Benouar D. Materials for the investigation of historical seismicity in Algeria from the records of past earthquakes. Annals of Geophysics. 2004;47(2-3). https://doi.org/10.4401/ag-3321
[5] D.T.R. (Document Technique Réglementaire) BC 2.48. Règles Parasismiques Algériennes RPA 99/V2003. 2004.
[6] D.T.R. (Document Technique Réglementaire) BC 2.48. Règles Parasismiques Algériennes RPA 2024. 2025.
[7] Abdelhamid A, Benahmed B, Laghrouche O, Palanci M, Aidaoui L. Evaluation of damping reduction factors for displacement and acceleration spectra using code-compatible near-fault and far-fault ground motions depending on site conditions. Research on Engineering Structures and Materials. 2025;11(1):213-230. https://doi.org/10.17515/resm2024.153ea0209rs
[8] Berra I, Boulaouad A. Algerian seismic code improvement by proposal of a specific design spectrum for Algiers City. Asian Journal of Civil Engineering. 2019;20:925–932. https://doi.org/10.1007/s42107-019-00154-w
[9] Koriga S, Ihaddoudene ANT, Saidani M. Numerical model for the non-linear dynamic analysis of multi-storey structures with semi-rigid joints with specific reference to the Algerian code. Structures. 2019;18:225–238. https://doi.org/10.1016/j.istruc.2019.01.008
[10] Fardis MN. Seismic design, assessment and retrofitting of concrete buildings based on EN-Eurocode 8. Berlin: Springer; 2018.
[11] Yadav P, Joshi R. Effect of height and position of shear wall on G+5 multi-storey building for zone III. International Journal of Recent Technology and Engineering. 2019;8(3):5452–5456. https://doi.org/10.35940/ijrte.C4609.098319
[12] Merabti S, Bezari S, Laari AA, Khachouche A. Investigation into the Impact of L-Shaped RC Shear Wall Placement with Openings on the Behavior of Medium-Rise Buildings. The Journal of Engineering and Exact Sciences. 2023;9(9):16816-01e. https://doi.org/10.18540/jcecvl9iss9pp16816-01e
[13] Merabti S, Guelmine L, Afkir M, Fekir Z. Numerical simulation of the behavior of L-shaped RC shear walls with staggered openings. Brazilian Journal of Production Engineering. 2024;10(3):164–173. https://doi.org/10.47456/bjpe.v10i3.45019
[14] Ahamad SA, Pratap K. Dynamic analysis of G+20 multi storied building by using shear walls in various locations for different seismic zones by using Etabs. Materials Today: Proceedings. 2021;43:1043–1048.
[15] FEMA-445. Next-Generation Performance-Based Seismic Design Guidelines. Federal Emergency Management Agency; 2006.
[16] Reshma T, Sankalpasri S, Tanu H, Nirmala M. Multistorey Building Analysis and Its Behavior because of Shear Wall Location Underneath Completely Different Seismal Zones. IOP Conference Series: Earth and Environmental Science. 2021;822(1):012044. https://doi.org/10.1088/1755-1315/822/1/012044
[17] Bhattacharjee J, Jain P, Gaurav A. Study the behaviour of high-rise buildings at different positions of shear walls subjected to seismic loading. International Research Journal of Science Engineering and Technology. 2017;6:64–75. https://doi.org/10.32804/RJSET
[18] Alothman A, Mangalathu S, Al-Mosawe A, Alam MM, Allawi A. The influence of earthquake characteristics on the seismic performance of reinforced concrete buildings in Australia with varying heights. Journal of Building Engineering. 2023;67:105957. https://doi.org/10.1016/j.jobe.2023.105957
[19] Boudina A, Benyamina S, Merabti S, Guettiche A, Chadouli R. Impact of several seismic scenarios on the dynamic responses of self-steady structures of different heights. Studies in Engineering and Exact Sciences. 2024;5(2):e11609. https://doi.org/10.54021/seesv5n2-629
[20] Chebihi A, Laouami N. Comparative seismic study between Algerian code (RPA99), European code (EC8) and American code (UBC97). In: Second European Conference on Earthquake Engineering and Seismology. Istanbul; 2014.
[21] Luo R, Lata A, Dong X, Wang B, Luo Z, Liang Y, et al. Seismic response of soft-story reinforced concrete frames: Challenging traditional collapse mechanisms. Structures. 2025;62:108894. https://doi.org/10.1016/j.istruc.2025.108894
[22] Koshiba Y, Nakayama J. Intentions of university students and staff members to re-enter chemical storage buildings immediately after a major earthquake: A case study in Japan. International Journal of Disaster Risk Reduction. 2021;61:102150. https://doi.org/10.1016/j.ijdrr.2021.102150
[23] Almayah AA, Taresh RG. Effect of Shear Wall Location on the Response of Multi Story Buildings Under Seismic Loads. International Journal of Scientific & Engineering Research. 2019;10(1):1303-1311.
[24] Guettiche A, Soltane MA, Lecheheb M, Boudina A. Seismic performance of historical unreinforced masonry buildings: The case of Souika district in Constantine, Algeria. Journal of Building Engineering. 2025;111:113377. https://doi.org/10.1016/j.jobe.2025.113377
[25] Soltane MA, Guettiche A, Khallef N, Lecheheb M. Seismic fragility assessment of Skikda's historic core: A comparative application of Risk-UE LM1 and LM2 frameworks. International Journal of Architectural Heritage. 2025. Advance online publication. https://doi.org/10.1080/15583058.2025.2577255
[26] D.T.R. (Document Technique Réglementaire) BC 2.2. Permanent loads and live loads. Algeria: National Center for Applied Research in Paraseismic Engineering; 1988.

[27] EN 1998-1:2004 (Eurocode 8): Conception et dimensionnement des structures pour leur résistance aux séismes. Comité Européen de Normalisation.
[28] Alinejad A, Majd GF, Zahrai SM. Impact of artificially seismic loading on the response of building structures using El Centro earthquake record as an input motion. Journal of King Saud University – Engineering Sciences. 2017;29(4):350–364. https://doi.org/10.1016/j.jksues.2017.06.002
[29] Ozmen HB, Inel M, Demirtas Y. Evaluation of different cases of soft story formation for mid-rise RC buildings. Research on Engineering Structures & Materials. 2020;6(3):229-240. https://doi.org/10.17515/resm2019.168ea1204
[30] Alrudaini T. Estimating vibration period of reinforced concrete moment resisting frame buildings. Research on Engineering Structures & Materials. 2023;9(4):1417-1432. https://doi.org/10.17515/resm2023.724st0331
[31] Ivanov I, Velchev D. Comparative Study of Different Linear Analysis for Seismic Resistance of Buildings According to Eurocode 8. Preprints. 2025 Mar 13. https://doi.org/10.20944/preprints202503.0930.v1
[32] Pashova L, Oynakov E, Paskaleva I, Ivanov R. Seismic Response Analysis of a Six-Story Building in Sofia Using Accelerograms from the 2012 Mw5.6 Pernik Earthquake. Applied Sciences. 2025;15(15):8385. https://doi.org/10.3390/app15158385
[33] Zheng H, Liu J, Wu J, Shi P, Ma W, Liu M. Rapid assessment of building losses in the M6.8 Tingri earthquake, Tibet, China. International Journal of Disaster Risk Science. 2025;16(3):408–432. https://doi.org/10.1007/s13753-025-00645-2
[34] Institute of Earthquake Forecasting, China Earthquake Administration. Procedures for Earthquake Scientific Investigation. In: A Guidebook to Earthquake Scientific Investigation. Springer; 2025. p. 13–16. https://doi.org/10.1007/978-981-96-0418-0_2
[35] Boulaouad A, Belagraa L, Bouglada MS. The Review of Algerian Building Seismic Code (RPA) in Seven Points Compared to American and European Codes. The Eurasia Proceedings of Science, Technology, Engineering & Mathematics (EPSTEM). 2021;13:45–50. https://doi.org/10.55549/epstem.1038424
[36] Milyardi R, Pribadi KS, Abduh M, Meilano I, Lim E, Hs H, et al. Rehabilitation and reconstruction cost drivers in earthquake-affected buildings: A damage-level-based analysis in Indonesia. Bulletin of Earthquake Engineering. 2025. Advance online publication. https://doi.org/10.1007/s10518-025-02243-5
[37] Demirci C, Málaga-Chuquitaype C, Macorini L. Seismic shear and acceleration demands in multi-storey cross-laminated timber buildings. Engineering Structures. 2019;198:109467. https://doi.org/10.1016/j.engstruct.2019.109467
[38] Lam N, Tsang HH, Li S. Inter-storey drift and storey shear forces in rocking isolated buildings. Structures. 2025;78:109274. https://doi.org/10.1016/j.istruc.2025.109274
[39] Şahin F, Turan FC. Comparison of 5 and 10 storey frame buildings and 5 and 10 storey shear wall-frame buildings under the effect of Maraş earthquake according to the Turkish Building Earthquake Code 2018. Journal of Civil Engineering and Urbanism. 2024;14(2):76–88. https://doi.org/10.54203/jceu.2024.6
[40] Merabti S, Guelmine L, Kaci M. Parametric analysis of the seismic behavior of reinforced concrete shear walls in buildings: Application of the pushover method. Romanian Journal of Materials. 2025;55(2).
[41] Khelladi M, Benyamina S, Merabti S. Influence of Empirical and Dynamic Periods on the Seismic Responses of Reinforced Concrete Buildings Braced by L-Shaped Shear Walls. The Journal of Engineering and Exact Sciences. 2024;10(4):18672. https://doi.org/10.18540/jcecvl10iss4pp18672